In Vivo Studies of HDL Assembly and Metabolism Using Adenovirus-Mediated Transfer of ApoA-I Mutants in ApoA-I-Deficient Mice†

Catherine A. Reardon,*,‡ Horng-Yuan Kan,§ Veneracion Cabana,‡ Lydia Blachowicz,‡ John R. Lukens,‡ Qingzhou Wu,‡ Kalliopi Liadaki,§ Godfrey S. Getz,‡ and Vassilis I. Zannis§

Department of Pathology, University of Chicago, 5841 S. Maryland Avenue, Chicago, Illinois 60637, and Section of Molecular Genetics, Whitaker Cardiovascular Institute, Boston University School of Medicine, 715 Albany Street, Boston, Massachusetts 02118-2394

Received July 12, 2001; Revised Manuscript Received September 10, 2001

ABSTRACT: We have used adenovirus-mediated gene transfer in apoA-I-deficient (A-I$^{-/-}$) mice to probe the in vivo assembly and metabolism of HDL using apoA-I variants, focusing primarily on the role of the C-terminal 32 amino acids (helices 9−10). Lipid, lipoprotein, and apoA-I analyses showed that plasma levels of apoA-I and HDL of the mutants were 40−88% lower than that of wild type (WT) human apoA-I despite comparable levels of expression in the liver. WT apoA-I and mutant 1 (P165A, E172A) formed spherical particles with the size and density of HDL_2 and HDL_3. Mutant 2 (E234A, E235A, K238A, K239A) generated spherical particles with density between HDL_2 and HDL_3. Mutant 3 (L211V, L214V, L218V, L219V) and mutant 4 (L222K, F225K, F229K), which have substitutions of hydrophobic residues in the C-terminus, generated discoidal HDL particles indicating a defect in their conversion to mature spherical HDL. Significant amounts of mutant 4 and mutant 5 (truncated at residue 219) were found in the lipid poor fractions after ultracentrifugation of the plasma (18 and 35%, respectively, of total apoA-I). These findings suggest that hydrophobic residues in and/or between helices 9 and 10 are important for the maturation of HDL in vivo.

Apolipoprotein A-I (apoA-I)[1] is the major protein constituent of HDL and plays an important role in HDL biogenesis, stability, and metabolism (*1*). The formation and catabolism of HDL are important in establishing its plasma level, although the details of both remain obscure. It is generally believed that three major anabolic processes contribute to the HDL levels: (a) de novo synthesis, especially of apoproteins A-I and A-II, by the liver and the intestine; (b) cholesterol efflux from peripheral tissues by the lipid-free or lipid-poor apoA-I forms; and (c) refashioning of HDL in plasma as a result of enzymatic activities and transfer proteins. Biogenesis of HDL is thought to occur primarily by the assembly of apoA-I with phospholipid, cholesterol, and other lipids to form initially phospholipid-rich discoidal particles of pre-β mobility. These particles are subsequently converted into spherical particles through the action of lecithin:cholesterol acyltransferase (LCAT) (*2*). As a component of HDL, apoA-I activates LCAT (*3*−*5*) and promotes the efflux of cholesterol from peripheral cells, thus providing a substrate for the LCAT reaction (*6*). It was recently shown that HDL cholesterol is provided by efflux of cellular cholesterol via the ATP-binding cassette transporter-A1 (ABC A1) gene (*7*−*9*). Mutations in the ABC A1 gene product that inhibit cholesterol efflux are associated with Tangier's disease and familial hypoalphalipoproteinemia. Biogenesis and catabolism of HDL are influenced by several other proteins (*10*).

There are at least three processes involved in the catabolism of HDL: (a) selective removal of cholesteryl ester from HDL mediated by scavenger receptor class BI (*11*), (b) removal of the intact HDL particle, and (c) the removal of lipid-poor apoA-I. The last two processes may involve the cubilin receptor, which recognizes both HDL and apoA-I (*12*, *13*). All these anabolic and catabolic processes contribute to the steady-state level of plasma HDL.

The amino terminal region of apoA-I (residues 1−43) is globular, whereas the carboxy terminal region (residues 44−243), which is encoded by exon 4, consists of either 22-mer or 11-mer repeating units, which are organized into 10 lipid binding amphipathic α-helices (*14*, *15*). Residues 190−243 (helices 8−10) have been shown to be important for lipid and HDL binding as well as for binding to cell membranes (*16*−*21*). Analysis of the lipid binding affinities of the apoA-I α-helices showed that helices 1 and 10 have higher lipid binding affinities than the other helices and that there is no cooperativity among adjacent helices for lipid binding (*16*, *22*). These sequences may be responsible for the initial association of phospholipids with apoA-I and thus play a

† This work was supported by NIH Grants HL57334 (to G.S.G) and HL 48739 (to V.I.Z.) and Biomed Grant BMH4-CT 98-3699 (to K.L.)

* To whom correspondence should be sent. Catherine A. Reardon, The University of Chicago, Department of Pathology, MC 1089, 5841 South Maryland Avenue, Chicago, IL 60637, Phone: (773) 702-2557. FAX: (773) 834−5251. E-mail: reardon@midway.uchicago.edu.

‡ University of Chicago.

§ Boston University School of Medicine.

[1] Abbreviations: A-I$^{-/-}$, apoA-I-deficient mice; A-I Tg, human apoA-I transgenic mice; ABC A1, ATP-binding cassette transporter A1; apo, apolipoprotein; CE, cholesteryl esters; FC, free cholesterol; HDL, high-density lipoprotein; HDL-C, HDL cholesterol; LCAT, lecithin cholesterol acyltransferase; PL, phospholipid; RID, radial immunodiffusion.

10.1021/bi011451e CCC: $20.00
Published on Web 10/12/2001

particularly vital role in HDL assembly. Essentially all prior in vivo studies of the role of the C-terminal portion of apoA-I have been confined to the analysis of deletions of various lengths of C-terminal residues (*23*−*25*). In this study, we have examined the role of charged and hydrophobic residues in the C-terminal helices in comparison with a deletion involving the last 23 amino acids. Our previous study (*26*) used apoA-I mutants with modifications in the putative helices 9 and 10 and the random coil that connects them, as defined by computer modeling and X-ray crystallography (*15*, *27*), to show that substitutions of Leu and Phe residues between positions 211 and 229 of apoA-I inhibited the binding of apoA-I to isolated plasma HDL in vitro as well as the initial association of apoA-I with multilamellar DMPC vesicles, indicating defects of apoA-I in phospholipid binding.

We have used adenovirus-mediated gene transfer in apoA-I-deficient (A-I$^{-/-}$) mice to investigate how different mutations in the apoA-I structure influence in vivo the level of plasma HDL and apoA-I, the nature of HDL species formed, and the percentage of lipid-free or lipid-poor apoA-I. In the current study, we examined the in vivo properties of four of the mutants involving modifications of the putative helices 9 and 10 and the connecting random coil used in the in vitro study (*26*), along with wild type (WT) apoA-I and an additional mutant that contains a change in helix 7 as a control for the mutants affecting the C-terminal domains. Our data indicate that mutations in apoA-I that inhibited binding to HDL and phospholipid in vitro also affected the levels of HDL in vivo. However, three of the mutants with similar defects in lipid binding in vitro, while unable to promote the formation of high levels of spherical HDL of normal subclass distribution, had subtle differences in the nature and level of HDL formed in vivo. These findings suggest that inferences drawn from the in vitro properties of apoA-I variants predict only some aspects of their behavior in vivo. They also suggest that more attention needs to be paid to the individual residues encompassed by helices 9 and 10 of apoA-I to fully understand the subtleties of HDL and apoA-I metabolism in vivo and that the efficient association of apoA-I with phospholipids and the ability of the resulting particles to promote cholesterol efflux and/or to efficiently activate LCAT are facilitative steps for the biogenesis and maturation of HDL.

EXPERIMENTAL PROCEDURES

Production of First Generation Recombinant Adenoviruses. A 1.8-kb genomic *Hin*dIII−*Bam*HI fragment containing the entire wild-type apoA-I gene coding sequence and flanking regions (from nucleotide 63 of exon 1 to 327 nucleotides downstream of exon 4) was excised from the pUC-AIgN plasmid (*10*) and cloned into the corresponding sites of pCA13 vector (Microbix Systems) to generate the pCA13-AIgN shuttle vector (Figure 1). This placed the coding sequence of the apoA-I gene under the control of the CMV promoter. To generate shuttle vectors containing the mutant apoA-I sequences, a region from the third intron to the 3′-flanking region of the wild-type apoA-I gene in the pCA13-AIgN vector was replaced by the corresponding regions in the mutant apoA-I gene sequences previously described (*26*). *Eco*RI fragments of 6 kb which encompass a 2.2-kb apoA-I gene sequence mutated at specific sites were

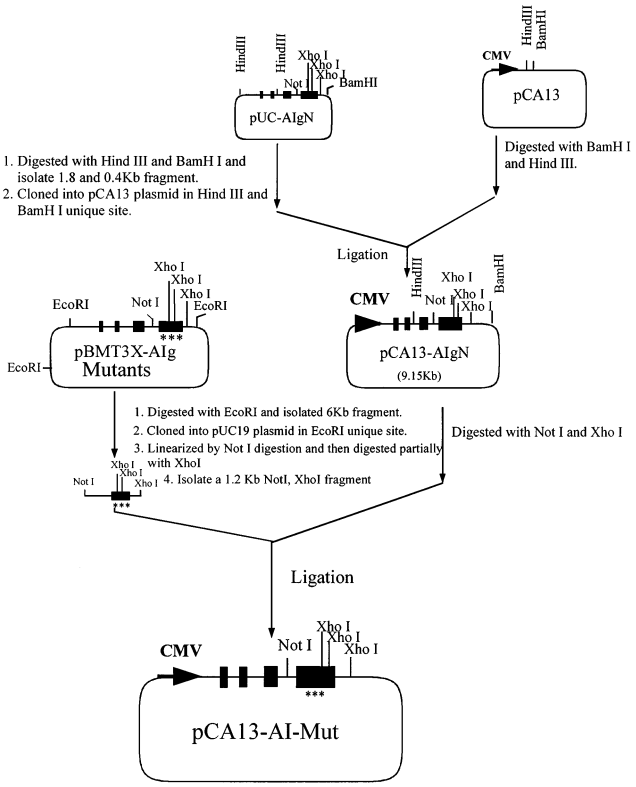

FIGURE 1: Cloning steps leading to the generation of recombinant wild-type and mutant apoA-I adenoviruses. The coding sequence of the gene for wild-type apoA-I was inserted into the adenovirus shuttle vector pCA13 to generate the pCA13-AIgN plasmid. A fragment of genomic DNA from the third intron to the 3′-flanking region containing the mutations M1 to M5 of Table 1 was used to replaced the wild-type gene sequence in the pCA13-AIgN plasmid. pCA13-A-I plasmids containing the wild-type gene or mutations M1-M5 along with a helper PJM17 adenovirus were used to transfect 293 cells to generate recombinant adenoviruses expressing the wild-type and the mutant apoA-I forms.

excised from the pBMT3X-AI vectors and cloned into the *Eco*RI site of pUC19 (New England Biolabs). The resulting plasmid was linearized with complete *Not*I digestion followed by partial *Xho*I digestion to release a 1.2-kb apoA-I gene sequence containing exon 4. This mutated apoA-I gene sequence was used to replace the wild-type sequence in the pCA13-AIgN shuttle vector. The mutant apoA-I gene sequences cloned into the pCA-13 vector were (i) P165A, Q172E; (ii) E234A, E235A, K238A, K239A; (iii) L211V, L214V, L218V, L219V; (iv) L222K, F225K, F229K; (v) P220 → Stop. The location of these mutations in the apoA-I helices as defined by computer modeling and X-ray crystallography is shown in Figure 2. pCA13-LacZ was generated by subcloning an *Eco*RI−*Bam*HI fragment from pCMV sport3-gal (Gibco-BRL) into the corresponding sites of pCA13. Recombinant adenoviral vectors were generated by cotransfection of the pCA13 plasmids containing the wild-type or mutant apoA-I gene sequences or LacZ along with the helper pJM17 adenovirus (Microbix System) into E1 transformed NIH-293 cells. The 293 cells were transfected using Dosper liposomal transfection reagent (Boehringer Mannheim) and overlayed with top agar (Gibco-BRL) containing 40 mM HEPES−HCl, pH 7.4, after 24 h. The isolated viral plaques containing the viruses obtained 1−2 weeks later were used to infect new P-60 dishes of 293 cells, and 72 h post-infection the media of the cells were analyzed

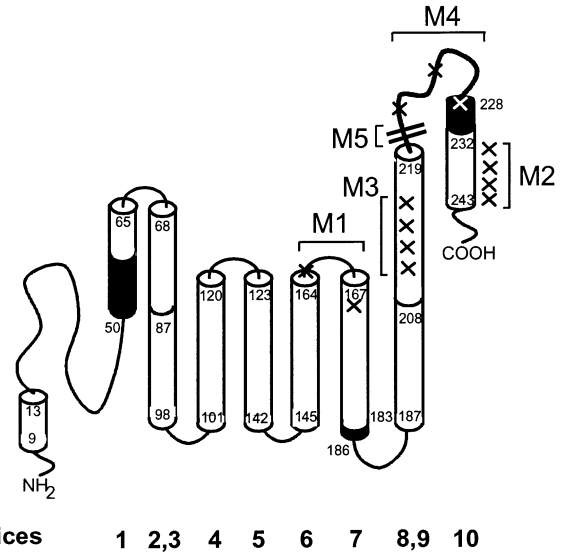

FIGURE 2: Model of the boundaries of the helical regions of apoA-I based on computer modeling (*15*) and X-ray crystallography (*27*). Cylinders represent amphipathic helices. Predicted amphipathic helices are shown in white; additional helical regions that were observed by X-ray crystallography are shown in black.

by SDS−PAGE and immunoblotting using anti-human apoA-I antibodies (Ottawa Heart Institute Research Company). In addition, cells were lysed with digestion buffer (10 mM Tris, pH 8.2, 0.4 M NaCl, 2 mM EDTA, and 1% SDS and 285 μg/mL proteinase K) 48 h post-infection and the DNA obtained from the cell lysates was analyzed by the polymerase chain reaction to identify positive plaques. All adenoviruses were subjected to three rounds of plaque purification using 911 cells prior to purification on two CsCl density gradients. The viruses were extensively dialyzed against filter sterilized 1× phosphate buffer (140 mM NaCl, 5 mM NaH_2PO_4, pH 7.8, 1.5 mM NaH_2PO_4) with the final dialysate containing 5% glucose. The titers of the viruses were generally between 1 and 5×10^{10} pfu/mL except mutant 4, which was 10-fold lower.

Animals. Male A-I$^{-/-}$ (ApoA1^{tm1Unc}) C57BL/6J mice (*28*) and human apoA-I transgenic mice (C57BL/6-TgN-(APOSA1)1 Rub) (*29*) were purchased from Jackson Laboratories (Bar Harbor, ME). The mice were maintained on a 12-h light/dark cycle and standard rodent chow. The mice were 10−14 weeks old at the time of injection of the adenoviruses. All procedures performed on the mice were in accordance with National Institutes of Health and institutional guidelines.

Adenovirus Injection and Analysis of Plasma. The A−I$^{-/-}$ mice were injected via the retro-orbital sinus with 5×10^8 pfu of recombinant adenovirus per animal. Each virus was injected into eight animals and the animals sacrificed three days post-infection. The only exception was the virus expressing mutant 5 (A-I Δ200−243), which was injected into only six mice. The liver was rapidly removed, divided into small pieces, and frozen in liquid nitrogen. The plasma from two animals was pooled and adjusted to 1mM PMSF, 0.2% aprotinin, 0.1% EDTA, and 0.002% Na azide prior to analysis and separation of lipoproteins. Plasma and lipoprotein lipid levels were determined using commercially available kits as described previously (*30*). All lipid analyses were performed by methods standardized against CDC furnished standards. The concentration of human apoA-I in the plasma and in the FPLC and equilibrium density gradient fractions was determined by radial immunodiffusion (RID) using a polyclonal antibody to human apoA-I (*30*). Standard human serum obtained from the Northwest Lipid Research Laboratory (Seattle, WA) was used as reference.

Fractionation of Plasma Lipoproteins. The lipoproteins in the plasma pools were separated by two methods. For gel filtration chromatography, 200−250 μL of the pooled plasma was fractionated on tandem Superose 6 FPLC columns (Pharmacia LKB Biotechnologies Inc.) in 0.2 M sodium phosphate, pH 7.4, 0.05 M NaCl, 0.03% EDTA, and 0.02% Na azide as described (*31*). For equilibrium density gradients, 150−250 μL of plasma was adjusted to 2 mL with PBS and the lipoproteins separated on 10−20% Na Bromide gradients (*31*). The fractions were dialyzed against 0.1 mM Tris, 0.9% NaCl, pH 8.0.

Immunoblotting. The FPLC fractions and dialyzed equilibrium density gradient fractions were subjected to electrophoresis on 10−20% SDS−PAGE (Novex). Following transfer to Immobilon-P (Millipore), the membrane was probed with polyclonal rabbit anti-human apoA-I antibodies (1:25 000 dilution) or rabbit anti-rat apoE antibodies (1:1000 dilution). Specific antibody binding was visualized by chemiluminescence (ECL, Amersham Corp.) using human serum adsorbed horseradish peroxidase coupled anti-rabbit IgG (Sigma). The relative intensities of the apoA-I and apoE signals were determined with NIH Image software after scanning the film using DeskScan II software.

Nondenaturing Gradient Gels. Fractions 12−25 from the equilibrium density gradient separation were pooled and subjected to nondenaturing gradient gel electrophoresis (*30*). Briefly, 5 μg of HDL protein (diluted 1:4 with 40% sucrose, 0.01% bromphenol blue) were applied to each lane of a 4−30% nondenaturing polyacrylamide gel (from David Rainwater, Southwest Foundation, San Antonio, TX). Proteins of known radii (High Molecular Weight Standards, Pharmacia) were included as standards: thyroglobulin, 8.5 nm; ferritin, 6.1 nm; catalase, 4.6 nm; lactate dehydrogenase, 4.1 nm; and albumin, 3.55 nm.

Electron Microscopy. Fractions 14 and 18 (for wild-type, M1 and apoA-I$^{-/-}$), fraction 17 (for M2), and fraction 18 (for M3−5) from density gradient centrifugation were dialyzed against ammonium acetate buffer (126 mM ammonium acetate, 0.26 mM EDTA, pH 7.4). Aliquots were stained with sodium phosphotungstate and examined in the Phillips CM-120 Electron Microscope (University of Chicago Electron Microscopy Laboratory) as previously described (*32*). The mean diameter of the particles was determined from photomicrographs taken at 200 000× magnification with between 140 and 400 particles measured per sample.

RNA Isolation and Northern Blotting. Total cellular RNA was isolated from liver using the Qiagen RNA/DNA Midi-Kit. Equal quantities of RNA (10 μg) were separated on 1.0% agarose-formaldehyde gels, transferred to Hybond-N+ nylon membrane (Amersham Pharmacia Biotech) and cross-linked to the filter by UV irradiation (Stratalinker, Stratagene). The apoA-I probe for hybridization contained 290 bp of exon 4 of human apoA-I and 148 bp of the intergenic sequence between the apoA-I and apoCIII genes. The mouse β-actin probe (184 bp) was obtained from Ambion (Austin, TX). Both probes were labeled with ^{32}P using the Multiprime

Table 1: Comparison of HDL-C, Plasma ApoA-I Levels and Hepatic ApoA-I Levels in Adenoviral Infected Mice[a]

recombinant adenoviruses used for infection of mice	HDL-C[b] mg/dL	ApoA-I[c] mRNA	plasma ApoA-I[d] mg/dL	lipid-poor ApoA-I[d] mg/dL (% total)
WT A-I	131 ± 8[g]	100%	323 ± 17[g]	36 (11%)
M1: A-I (Pro^{165} → Ala, Gln^{172} → Glu)	69 ± 7[e,g]	150%	192 ± 23[e,g]	12 (6%)
M2: A-I (Glu^{234} → Ala, Glu^{235} → Ala, Lys^{238} → Ala, Lys^{239} → Ala)	44 ± 6[e,g]	101%	143 ± 26[e,g]	6 (4%)
M3: A-I (Leu^{211} → Val, Leu^{214} → Val, Leu^{218} → Val, Leu^{219} → Val)	39 ± 4[e,g]	235%	114 ± 16[e,g]	11 (10%)
M4: A-I (Leu^{222} → Lys, Phe^{225} → Lys, Phe^{229} → Lys)	19 ± 3[e]	108%	36 ± 11[e]	6 (18%)
M5: A-I (Pro^{220} → Stop)	26 ± 4[e]	115%	48 ± 13[e]	17 (35%)
LacZ	23 ± 2[e]	nd	0	0
A-I$^{-/-}$ (not infected)	15[e]	nd	0	0
A−I Tg (not infected)	85[f,g]	nd	271[g]	16 (6%)

[a] Plasma obtained from mice was analyzed for HDL cholesterol (HDL-C) and human apoA-I levels (mean ± SEM). Liver human apoA-I mRNA levels are expressed relative to that in mice infected with wild-type apoA-I virus. The amount of lipid poor apoA-I (mg/dL) was determined from the percent of total apoA-I in the lipid-poor fractions on equilibrium gradients (% total) (Figure 3) and the plasma apoA-I levels (mg/dL). (nd = not determined). [b] $n = 4$ except $n = 3$ for mutant 5 and $n = 1$ for uninfected A-I$^{-/-}$ and apoA-I Tg mice. [c] $n = 2$ except $n = 1$ for M1. [d] $n = 4$ except $n = 3$ for mutant 5 and $n = 1$ for apoA-I Tg. [e] $p < 0.0001$ vs wild-type apoA-I expressing mice. [f] $p < 0.05$ vs wild-type apoA-I expressing mice. [g] $p < 0.05$ vs LacZ expressing mice.

DNA Labeling System (Amersham Pharmacia Biotech). Quantitation of X-ray film was performed by a phosphorimager (Molecular Dynamics) using the ImageQuant program. The apoA-I mRNA signal was normalized for the β-actin mRNA signal.

Generation, Purification, and In Vitro Studies of Mutant 5 (A-I Δ220−243). The ability of mutants 1−4 to bind to DMPC multilamellar liposomes and activate LCAT activity was previously determined (*26*). To examine these properties of mutant 5, stable mouse mammary tumor C127 cell lines expressing mutant 5 were generated and large-scale growth of cells and purification of the protein from the culture media of cells by ion-exchange chromatography by gel filtration was performed as described previously (*26*). The binding of the wild-type and the mutant 5 of apoA-I to DMPC multilamellar liposomes was studied by kinetic-turbidimetric methods as described (*26*). LCAT activity was measured using rHDL and purified human LCAT enzyme (*26*). The reaction was carried out for 30 min at 37 °C.

Statistics. Results are expressed as mean ± SEM. Statistical analysis was performed using StatView 5.01 software. Results were analyzed by one-way analysis of variance (ANOVA). Significance level was set at $P < 0.05$.

RESULTS

Plasma Lipids, HDL-C, and ApoA-I Levels and Hepatic ApoA-I mRNA Levels Following Adenoviral Infection. A-I$^{-/-}$ mice were infected with adenoviruses encoding wild-type or mutant human apoA-I or LacZ at a dose of 5×10^8 pfu per animal, and plasma was sampled 3 days after viral infection. A-I$^{-/-}$ mice were used to avoid competition between transferred human apoA-I and endogenous murine apoA-I. The concentration of virus and the time of analysis were selected following preliminary experiments in which we examined the lipoprotein profile and the decay of apoA-I expression in mice infected with wild-type apoA-I virus. To ascertain that adenoviral infection of mice had not induced an acute phase response or a profound liver toxicity, the plasma of each animal was monitored for serum amyloid A protein and transaminase activity, respectively. The concentration of neither of these proteins was significantly elevated (data not shown).

In these studies, we have examined four mutants of apoA-I in which changes were introduced into helices 9 and 10 and the connecting random coil (M2-M5). As controls, we also infected animals with adenoviruses carrying the wild-type apoA-I sequences and a mutation affecting helix 7 (M1). Lipid and human apoA-I levels in the plasma 3 days post-infection are shown in Table 1. HDL-cholesterol (HDL-C) levels ranged from 15 mg/dL in the uninfected A-I$^{-/-}$ mice to 131 mg/dL in mice expressing wild-type apoA-I. Plasma apoA-I levels ranged from 36 to 323 mg/dL with the highest level expressed by the animals infected with adenovirus expressing wild-type apoA-I. ApoA-I levels in the mice infected with wild-type apoA-I adenovirus were only slightly higher than in the human apoA-I transgenic mice. There was a strong positive correlation between HDL-C and plasma apoA-I level ($r^2 = 0.8422$).

One possible explanation for the differences in the plasma levels of the apoA-I proteins could be differences in the expression of the wild-type and mutant apoA-I forms. Since the liver is the primary site of adenovirus infection (*33*), RNA obtained from the liver at the time of euthanasia was analyzed by Northern blotting for the level of human apoA-I mRNA. As shown in Table 1, the relative level of the mRNA obtained from the liver of mice infected with the adenoviruses encoding the apoA-I mutants was comparable to or higher than that of mice infected with the wild-type apoA-I. In experiments not shown, wild-type apoA-I and the mutant proteins were synthesized and secreted into the media with equal efficiency by cultures of rat hepatoma cells (McA RH7777) infected with the viruses. In addition, permanent C127 cells expressing the mutant proteins M1-M4 were previously found to secrete the proteins at levels comparable to the wild-type protein (*26*). Thus, the differences in the plasma levels of the proteins most likely represent differences in the formation and/or catabolism of the HDL particles containing the different mutant apoA-I proteins in vivo.

Since infection with the apoA-I-expressing adenoviruses resulted in increased plasma apoA-I and HDL-C, this potentially could influence the distribution of other apoproteins, perhaps as a result of competition for available lipid. To assess this, the lipoprotein distribution of endogenous apoE, which is present on the HDL in A-I$^{-/-}$ mice, in animals

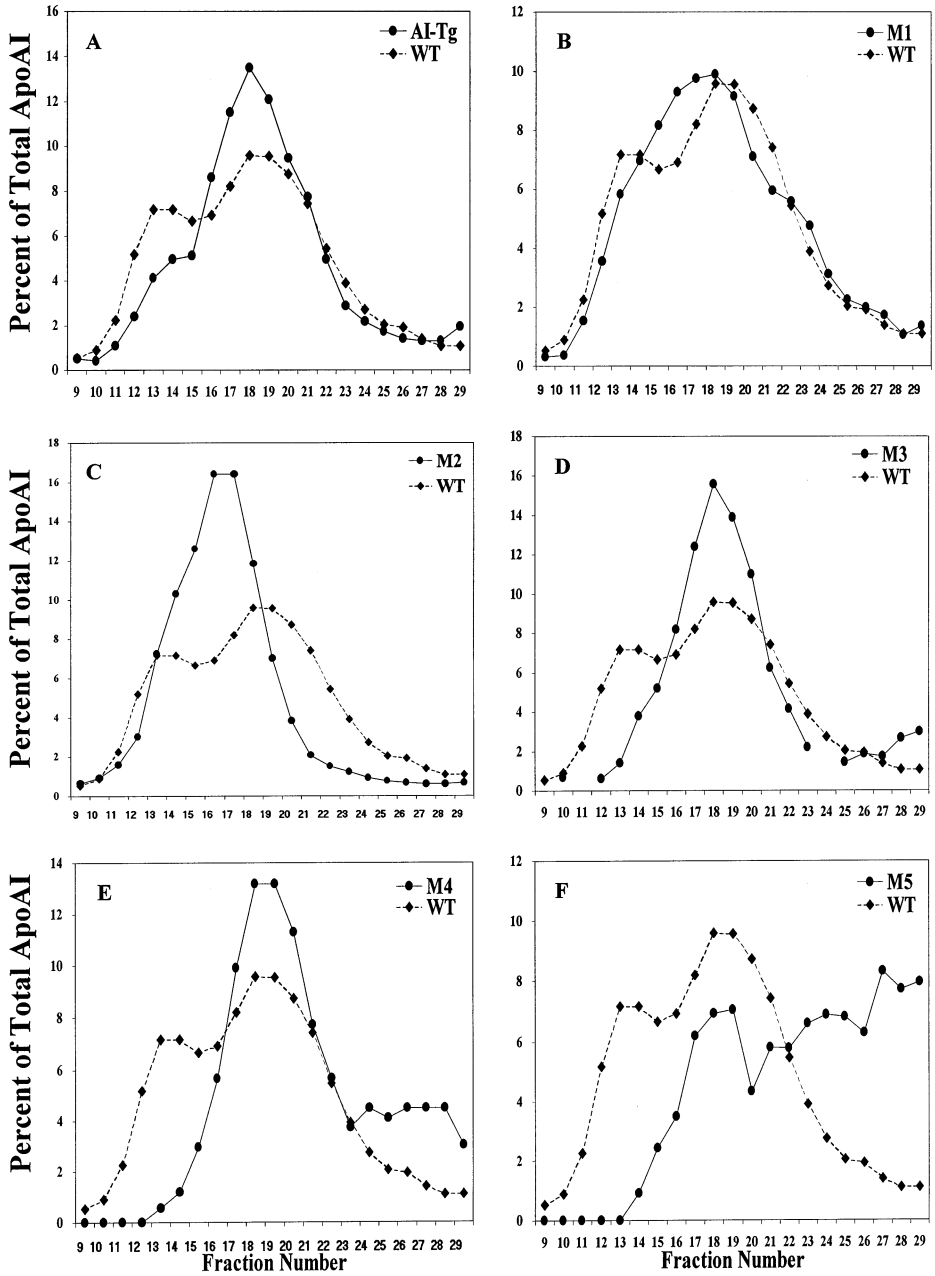

FIGURE 3: Distribution of apoA-I proteins on HDL fractions obtained by equilibrium density gradient centrifugation of plasma. A-I$^{-/-}$ mice were infected with a dose 5×10^8 pfu of recombinant adenoviruses and the plasma isolated 3 days post-infection. Plasma was also obtained from human apoA-I transgenic mice. The plasma was separated by equilibrium density gradient and the concentration of apoA-I protein in each fraction was determined by RID as described in the Experimental Procedures. The amount of apoA-I in each fraction is expressed as percent of total apoA-I in all fractions. The distribution of apoA-I from mice infected with adenovirus expressing the wild-type apoA-I is shown on each graph for comparison. A representative distribution for each apoA-I proteins is shown. ($n = 4$ except M5 where $n = 3$ and apoA-I Tg where $n = 1$).

expressing the various apoA-I proteins was determined by immunoblotting. No differences in the distribution of this protein were observed (data not shown).

Effect of the Mutations on the Nature of HDL in the Plasma. The plasma samples were fractionated by equilibrium density gradient centrifugation (Figure 3) and by gel filtration by FPLC (Figure 4) to examine the distribution of the human apoA-I proteins on HDL and to assess the stability of association of apoA-I with the HDL particles. Centrifugation provides the best assessment of the distinction among HDL subclasses and requires more stable association of the apoprotein with HDL for it to remain associated with the lipoprotein particles than does FPLC. This allowed us to obtain evidence as to what extent apoA-I exists as lipid-free/lipid-poor apoprotein for each mutant (Table 1). The effects of the apoA-I mutations on HDL distribution and the percentage of lipid-free/lipid-poor apoA-I are presented separately for the wild type and the different mutant forms of apoA-I.

Wild-Type ApoA-I. In mice infected with wild-type apoA-I, the denser, smaller HDL_3 particles accounted for ~60% of the total HDL, while in the transgenic mice HDL_3 was the major HDL subclass (~75%) (Figure 3). This was also evident in the FPLC profiles of the same samples, where the subclasses are not as readily separated (Figure 4). Relatively little lipid-free/lipid-poor apoA-I was seen in either

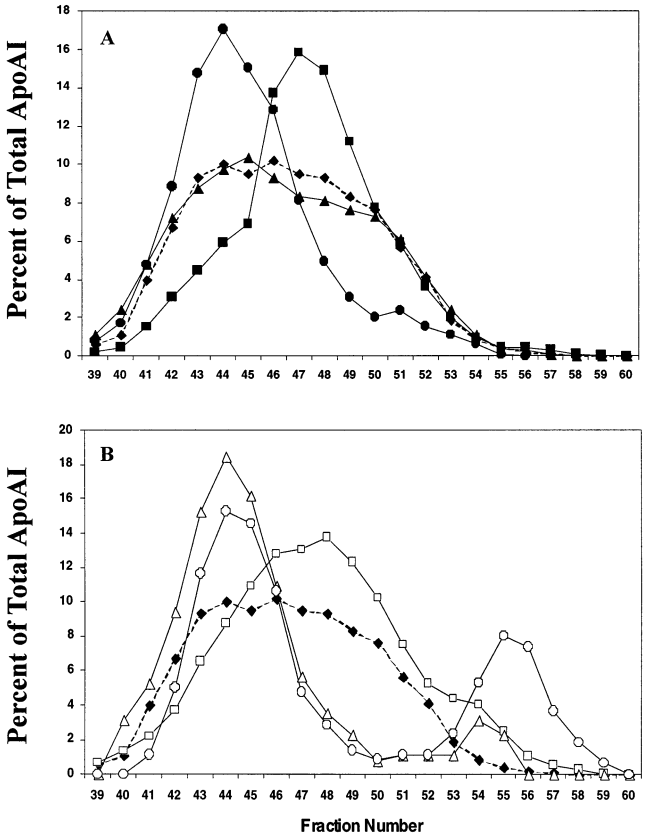

FIGURE 4: Distribution of apoA-I proteins in FPLC fractions. Aliquots of the plasma used in Figure 3 were separated on tandem Superose 6 columns. The amount of apoA-I in each fraction is expressed as a percent of total in all fractions. (A) WT apoA-I (♦), A-I Tg (■), M1 (▲), and M2 (●). (B) WT apoA-I (♦), M3 (□), M4 (△), and M5 (○). A representative distribution for each apoA-I protein is shown. ($n = 4$, except M5 where $n = 3$ and apoA-I Tg where $n = 1$)

the density gradient (≥ fraction 27) or the FPLC (≥ fraction 54) profiles. When the lipoproteins from both the transgenic and adenovirus-infected mice expressing wild-type apoA-I were examined by nondenaturing gel electrophoresis (Figure 5), two major discrete peaks of HDL were observed with Stokes' radii of 5.6 and 4.7 nm. A third minor peak of smaller lipoprotein particles with radii of 3.9 nm was seen also in these samples. By this procedure, the predominance of the small HDL particles was particularly evident, especially in the transgenic animals. Electron microscopy revealed mostly spherical HDL particles (Figure 6). Around 2% of the HDL_2 particles in mice infected with wild-type apoA-I adenovirus were discoidal.

Mutation in Helix 7. Mutant 1 (P165A, Q172E). In mutant 1 (M1), the proline helix breaker between helices 6 and 7 was replaced by an alanine, while the substitution of glutamine by a glutamic acid was introduced to convert a type A to type B half helix (*26*) (Figure 2). The HDL-C and plasma protein levels of M1 were about 60−70% of that of mice infected with the wild-type apoA-I (Table 1). The HDL subfractions containing this apoA-I variant had a distribution very similar to that seen with wild-type human apoA-I, whether examined by FPLC (Figure 4), density gradient centrifugation (Figure 3), or nondenaturing gel electrophoresis (Figure 5). Similar to wild-type apoA-I, the majority of this mutant was also associated with HDL (Table 1), and the particles were spherical (Figure 6). The HDL_2 and HDL_3

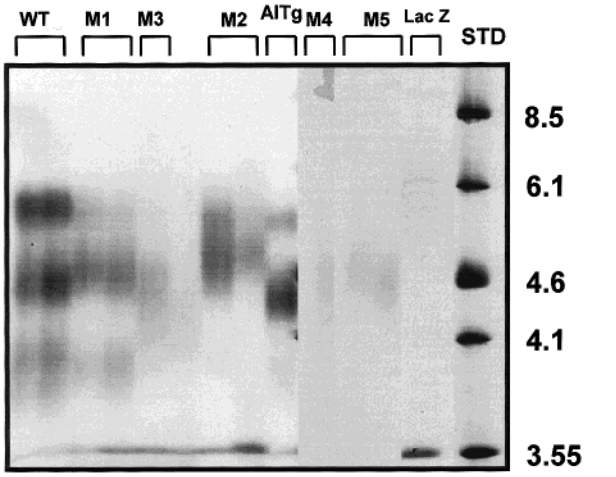

FIGURE 5: Nondenaturing gradient polyacrylamide gel electrophoresis. Aliquots of HDL peak fractions from equilibrium density gradient centrifugation were pooled and lipoproteins separated on 4−30% nondenaturing gradient gels as described in the Experimental Procedures. The Stokes' radii of the molecular weight standards (std) in nm is shown on the right.

from the peak fractions from the density gradient containing mutant 1were slightly, but significantly, smaller in diameter on negative staining electron microscopy than the particles from the corresponding fractions obtained from mice expressing wild-type apoA-I (Table 2).

Mutants of Helices 9 and 10. The remaining four mutants affect helices 9 and 10 and the random coil that connects them. The results of these changes are reported below in the order of their increasing disruption of HDL metabolism.

(a) Mutant 2 (E234A, E235A, K238A, K239A). In mutant 2 (M2), glutamic acid residues at positions 234 and 235 and lysine residues at positions 238 and 239 in helix 10 were each replaced by alanine residues (Figure 2). The mean levels of both HDL-C and apoA-I were about 40−45% of that seen in the animals expressing wild-type human apoA-I (Table 1). Upon density gradient centrifugation of the plasma, apoA-I was distributed broadly with a peak between the HDL_2 and HDL_3 subclasses (Figure 3). On the other hand, when examined by FPLC (Figure 4), most of the apoA-I was found in the large HDL fractions (peak fraction 44), with a relatively monodisperse distribution. These observations are compatible with the nondenaturing gradient gel electrophoresis (Figure 5), which showed a broad sized distribution of lipoprotein between the positions of HDL_2 and HDL_3, with no evidence of the smaller particles seen in mice expressing wild-type apoA-I or mutant 1. These particles were also spherical (Figure 6).

(b) Mutant 3 (L211V, L214V, L218V, L219V). Mutant 3 (M3) contains a conservative substitution of four leucine residues in helix 9 with valine residues (Figure 2). In animals infected with an adenovirus expressing mutant 3, there was a modest 1.5−2-fold increase in HDL-C as compared to mice injected with the control LacZ virus. The concentration of apoA-I was about 35% of that observed in animals expressing wild-type apoA-I. Almost all of the apoA-I eluted in fractions corresponding to the smaller, denser HDL_3 whether examined by equilibrium gradient centrifugation (Figure 3) or FPLC (Figure 4). The mobility of these particles on nondenaturing gradient gel electrophoresis (Figure 5) was similar to HDL_3,

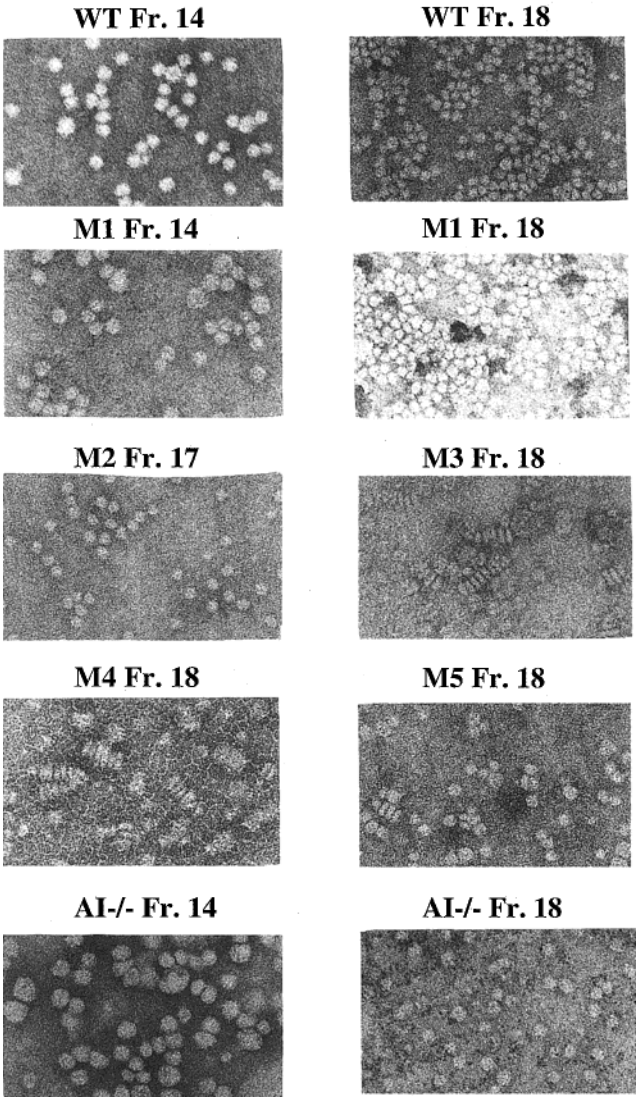

FIGURE 6: Electron photomicrograph of negatively stained HDL from adenovirus infected mice. HDL was separated by equilibrium density gradient centrifugation. The indicated aliquots of the peak HDL fractions were examined by electron microscopy as described in Experimental Procedures. The photomicrographs were taken at 100× magnification and enlarged 2.9× (100 nm = 29 mm).

but they were largely discoidal by electron microscopy (Figure 6).

(c) Mutant 4 (L222K, F225K, F229K). In mutant 4 (M4), three hydrophobic residues in the random coil connecting helix 9 and 10 were converted to positively charged residues. In animals infected with an adenovirus expressing mutant 4, HDL-C did not rise above the levels seen in mice infected with the control LacZ virus, and plasma apoA-I levels were approximately 10% of those seen in mice expressing the wild-type apoA-I containing virus. The distribution of apoA-I differs depending whether the lipoproteins were separated by FPLC or density gradient centrifugation. Most of the apoA-I eluted with the larger HDL particles (fractions 41−47) on FPLC (Figure 4), but in dense fractions (fractions 16−22) on density gradient centrifugation (Figure 3). On nondenaturing gradient gel electrophoresis, the stainable HDL protein was broadly distributed primarily around the size range of the HDL_3 particles (Figure 5). Similar to M3, these particles were also largely discoidal (Figure 6). Both M3 and M4 have lower CE:PL+FC ratio as compared to HDL from mice expressing wild-type apoA-I and the other mutants (Table 2). This is indicative of a lack of core lipids and is consistent with the discoidal nature of the particles. Unlike the other mutants described so far, a significant amount of M4 protein was detected in the lipid-free/lipid-poor fractions.

Table 2: Radii and CE:PL+FC Content of HDL Particles[a]

ApoA-I	radii (nm)	CE:PL+FC
WT A-I (fr. 14)	5.92 ± 0.05	1.6
M1 (fr. 14)	5.63 ± 0.04[b]	1.1
A-I$^{-/-}$ mice (fr. 14)	5.80 ± 0.07	0.5
WT A-I (fr. 18)	4.48 ± 0.04	1.5
M1 (fr. 18)	3.88 ± 0.05[c]	1.1
M2 (fr. 17)	4.55 ± 0.07	1.9
M3 (fr. 18)	5.91 ± 0.09	0.1
M4 (fr. 18)	5.76 ± 0.09	0.1
M5 (fr. 18)	5.47 ± 0.07[c]	0.4
A-I$^{-/-}$ mice (fr. 18)	5.30 ± 0.06[c]	0.7

[a] The radii (mean ± SEM) of the HDL were determined from the negative stain EM of the individual HDL fractions from equilibrium density gradient as described in Figure 6. Between 140−400 particles were measured for each sample. The statistical significance of the difference in size of the spherical particles (i.e., M1, M2, M5, and A-I$^{-/-}$) was compared to the corresponding fraction from wild-type apoA-I expressing mice. [b] $p \leq 0.0001$ versus wild-type apoA-I fraction 14. [c] $p \leq 0.0001$ versus wild-type apoA-I fraction 18. The aliquots used for EM were also analyzed for PL, FC, and CE content. The results are expressed as a ratio of CE:PL +FC to provide an indication of the core:surface lipid ratios.

(d) Mutant 5 (C Terminal Truncation at Position 220). In mutant 5 (M5), a stop codon was introduced at residue 220 which removed the C-terminal helix (helix 10) and the random coil connecting helices 9 and 10. The plasma apoA-I levels of this mutant were only 15% of that seen in mice infected with the wild-type apoA-I. HDL-C levels were slightly higher than those observed in mutant 4 (Table 1) and its distribution was similar to that of mutant 4, with M5 protein found in large HDL particles upon separation by FPLC (Figure 4), but in denser or small particles upon centrifugation (Figure 3) and on nondenaturing gradient gel electrophoresis (Figure 5). A larger percentage of mutant 5 apoA-I was also found in the lipid-free/lipid-poor fractions as compared to all of the other proteins: almost 35% after density gradient centrifugation (≥ fraction 27 in Figure 3) and 12% upon FPLC fractionation (≥ fraction 54 in Figure 4). We calculated the absolute amount of the different apoA-I mutants present in the lipid-free/lipid-poor fractions after density gradient centrifugation based on the percentage of total apoA-I in fractions 27−29 and the total amount of plasma apoA-I (Table 1). Only wild-type apoA-I had more apoA-I in the lipid-free/lipid-poor fractions than mutant 5. With this mutant, the particles examined from the HDL_3 peak were predominantly spherical with only 4% being discoidal (Figure 6). It is possible that the discoidal particles observed represent particles containing mutant 5 apoA-I, since no discoidal particles were observed in the HDL_3 density range of the A-I$^{-/-}$ mice.

Mutant 5 Has Reduced Ability to Activate LCAT and to Bind Multilamellar DMPC Vesicles in Vitro. Since the in vitro properties of M5 were not previously characterized (*26*), the LCAT activation potential of M5 was examined. Figure 7A shows that the ability of this mutant to activate LCAT was 38% of that of the wild type recombinant pro-apoA-I

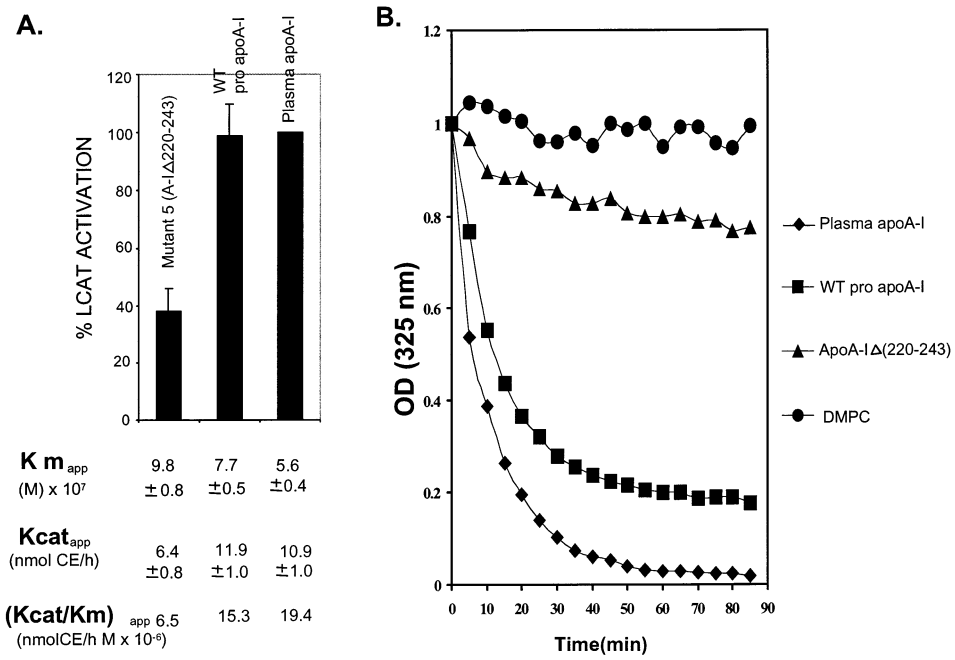

FIGURE 7: Phospholipid binding and LCAT activation properties of mutant 5 (apoA-I Δ220−243) and WT apoA-I. (A) LCAT activation by M5, wild-type recombinant pro-apoA-I, and plasma apoA-I. The LCAT activity was assayed as the rate of production of labeled cholesterol esters from the rHDL vesicles, as described in Experimental Procedures. The labeled cholesterol esters were separated from the free cholesterol by thin-layer chromatography. All LCAT assays were standardized by adding fixed amounts of apoA-I (reconstituted in the HDL particles), and LCAT enzyme. Error bars represent standard deviation for $n = 3$ or $n = 4$ experiments. The kinetic parameters for each of the apoA-I proteins assayed are shown below their respective bars in the graph. (B) Solubilization of multilamellar vesicles of DMPC by wild type and M5 apoA-I forms, monitored by the turbidity change as a function of time, at 24 °C. Multilamellar vesicles of DMPC were combined with wild-type recombinant or plasma apoA-I or M5 at a ratio of DMPC/apoA-I of 2.5:1 (w/w). The change in turbidity was monitored by the change in absorbance at 325 nm, at 5 min intervals, and was plotted as a function of time.

and plasma apoA-I. The apparent catalytic efficiency ($(k_{cat}/K_m)_{app}$) of M5 was reduced approximately 3-fold as compared to the wild-type proapoA-I and plasma apoA-I. This was the result of an increase in the apparent K_m and a decrease in the apparent K_{cat} of M5. DMPC binding experiments were performed also to assess the effect of the mutation on the kinetics of interaction of apoA-I with DMPC multilamellar vesicles at 24 °C. As illustrated in Figure 7B, while plasma and recombinant wild-type proapoA-I bind and solubilize DMPC rapidly, as indicated by the dramatic decrease in turbidity of the DMPC dispersions, M5 interacts very slowly with the phospholipid.

DISCUSSION

In this study, we have examined a number of mutants involving specific amino acid substitutions or truncations between residues 211 and the C-terminus of human apoA-I. The helices in this domain have been shown to have high lipid binding capacity and to be responsible for the initial penetration of the phospholipid layer (*16*, *22*). Several previous studies have indicated that deletion of the C-terminal region of apoA-I decreases its association with HDL and increases the rate of its catabolism in the plasma (*23*−*25*). We have asked how mutants bearing point mutations in this domain influence HDL formation and metabolism in vivo. The behavior of these apoA-I mutants was compared with wild-type apoA-I, a double point mutation affecting helix 7, and a truncation mutant lacking the last 23 amino acids of apoA-I. The in vitro properties of these mutants with respect to their capacity to associate with plasma HDL, to activate LCAT, and to solubilize DMPC vesicles have been analyzed previously (*26*) or in the present study (Figure 7). At issue in the current study is how these variants of apoA-I affect HDL metabolism in vivo. Overall, analysis of the in vitro and in vivo properties of the apoA-I mutants indicate that mutations in apoA-I that retain the capacity of apoA-I to bind to phospholipids are generally associated with relatively high apoA-I and HDL levels and form spherical HDL particles. In contrast, two of the mutations (M4 and M5) that affect the binding of apoA-I to phospholipids have relatively low apoA-I and HDL levels. Mutations M3, M4, and possibly M5 form discoidal particles. These findings suggest that mutations that exhibit reduced ability of apoA-I to solubilize multilamellar phospholipid vesicles in vitro are defective in the biogenesis of HDL in vivo, preventing, as in the case of M3 and M4, the conversion of the discoidal to spherical HDL particles (Figure 8).

Undoubtedly, the metabolism of HDL and apoA-I in these mice is complex. All measurements were made at a single time point, 3 days after viral infection, so that the mass measurements of apoA-I are the net result of the rates of catabolism, assuming that production rates are similar. In the case of HDL and apoA-I, their level is the net result of lipid association of apoA-I, lipid transfer, esterification by LCAT, and catabolism of various particles and lipid-free/lipid-poor apoA-I. As adenovirus injected intravenously is largely targeted to the liver, we expect very little of the apoA-I appearing in the plasma to have originated from nonhepatic tissues. While we cannot exclude variations in the production rate of HDL in vivo as a function of the structure of apoA-I expressed, we believe that the preponderance of evidence favors metabolic mechanisms to explain

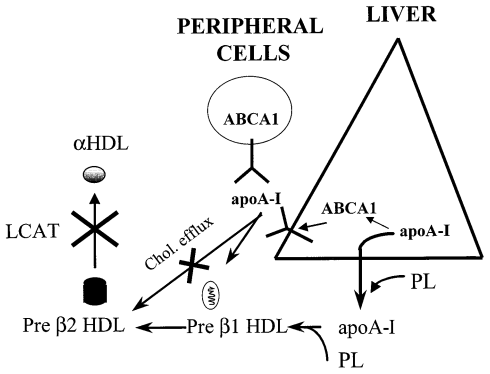

FIGURE 8: Schematic representation showing defective biogenesis of HDL in vivo involving defects in the ability of apoA-I mutants to promote cholesterol efflux, perhaps due to defective interaction with ABC A1, and/or activation of LCAT that may account for the inability of some of the mutant apoA-I proteins to produce spherical HDL particles. See discussion for details.

the variations in the levels of HDL-C and apoA-I in these experiments. There was no correlation between hepatic apoA-I mRNA levels and plasma apoA-I levels. On the basis of their expression in cultured cells (26 and data not shown), it appears that the capacity of the liver to secrete wild-type apoA-I and the mutants is equivalent. Thus, we attribute the differences in plasma levels to variations in the peripheral phases of HDL metabolism. The precise aspects of the peripheral metabolism of HDL that account for these concentration differences are not clarified by this study.

Among the mutant apoA-I forms studied here, those that associate with HDL in vitro and clear DMPC vesicles (*26*) were also capable of forming mature HDL particles in vivo. This included wild-type apoA-I, mutant 1 which affects helix 7 and the mutant 2 where the C-terminal charged residues at positions 234, 235, 238, 239 were replaced by alanines. Although all three apoproteins produced spherical particles, albeit with some minor differences in subclass distribution, their plasma expression level varied somewhat with wild-type apoA-I exhibiting the highest plasma apoA-I level and mutant 2 the lowest level of the three. The fact that mutant 1 (helix 7) and mutant 2 (helix 10) are capable of forming spherical particles in vivo suggests that they are able to efficiently activate LCAT in vivo. Mutant 1 was 60% as effective at activating LCAT in vitro as was wild-type apoA-I, and this level of activation appears to be sufficient to support the development of a cholesteryl ester core in HDL (Table 2). Mutant 2 also forms spherical particles containing a cholesteryl ester core. This mutation involves changing four of the six charged residues in the C-terminal helix 10 of apoA-I to alanine. Using mostly deletion mutagenesis (*23*−*25*) and isolated peptides representing each of the amphipathic helices (*16*, *22*), evidence indicates that the C-terminal helices, and especially helix 10, are critical for high affinity lipid or lipoprotein association. However, the four charged residues changed in mutant 2 do not appear to be critically required for this property. The belt model for discoidal HDL suggests that A/B dimer containing two antiparallel apoA-I chains wraps around the disk (*27*, *34*−*36*). In the belt model, the carboxyl-terminal apoA-I helix appears to be important for dimer formation on the HDL particle. The belt model assumes that intermolecular charge interactions of the dimer are optimized on the surface of the discoidal particles. The charge interactions between juxtaposed residues E235 and E234 on helix A with K239 and K238 on helix B contribute to the stability of the antiparallel helices on the surface of the discoidal HDL particles (*36*). Such interactions would be reduced in mutant 2.

On the other hand, the other three mutants (M3, M4, and M5) inefficiently solubilize phospholipids and do not bind to HDL in vitro (26 and Figure 7B). Upon the basis of these findings, one might expect that these mutants may be defective in the biogenesis of plasma HDL. Although expressed at different levels, both mutants 3 and 4 formed predominantly discoidal particles when expressed in apoA-I$^{-/-}$ mice. Mutant 3 has substitutions of valines for four leucines in helix 9, three of which are highly conserved (*37*), and is expressed at higher levels than mutant 4. Mutant 4 also involves substitution of hydrophobic residues, but in this case nonconserved substitutions in the interhelical region between helices 9 and 10 (*37*). These findings suggest that the mutations in helix 9 and 10 and the random coil connecting them blocks the maturation of discoidal to spherical HDL particles. This interpretation is consistent with the low CE:FC+PL ratio of the these particles (Table 2). These results point to the importance of the leucine residues in helix 9 of the apoA-I molecule, and the critical role of three hydrophobic residues in the random coil between helices 9 and 10 for the formation of mature HDL.

Three major in vivo processes that may affect HDL biogenesis and catabolism are (a) the ability of apoA-I to associate initially with phospholipid, (b) the ability of apoA-I to recruit cholesterol and phospholipid, especially from peripheral cells via ABC A1, and (c) the ability of apoA-I to activate LCAT (Figure 8). The preponderance of discoidal HDL in animals expressing mutants 3 and 4 suggests that either LCAT activation is impaired or the maturation of HDL to form spherical particles mediated by ABC A1 may be highly inefficient in these mice. Despite the relatively good LCAT activation achieved by mutant 3 in vitro using reconstituted HDL as a substrate (68% as compared to wild-type apoA-I and as effective as mutant 1 which does form spherical cholesteryl ester containing particles in vivo) (*26*), this mutant may not support high LCAT activation in vivo. Alternatively, this mutant may interfere with cholesterol efflux from peripheral cells and diminish the concentration of the LCAT substrate in the plasma of A-I$^{-/-}$ mice expressing this mutant. Although the sequences of apoA-I that interact with or mediate cholesterol efflux involving ABC A1 have not yet been identified, previous studies have shown that residues 209−243 appear to be important for lipid-poor apoA-I mediated cholesterol and phospholipid efflux (*38*). The leucine residues between amino acids 211−219 that are changed in mutant 3 may participate in a leucine zipper-type interaction among amphipathic helices, or they may be involved in the microsolubilization of membranes by facilitating insertion of the α-helices between the phospholipids, which may facilitate lipid efflux. Clearly, valine does not meet the functional role of leucine in these highly conserved positions. Mutant 4 also has amino acid substitutions within this region which may impact on ABC A1-mediated cholesterol efflux as well.

In mutant 4, three hydrophobic residues (Leu 222, Phe 225, Phe 229) were changed to lysines. This mutant of apoA-I is capable of forming a stable helical structure in the lipid-free state (*39*). The plasma levels of this mutant

were the lowest of all the mice infected with the different apoA-I proteins in the present study. The in vitro LCAT activation ability of this mutant was only 38% of the wild-type apoA-I, and this may account for the absence of core lipids in the HDL containing this mutant (Table 2). It is not clear whether the behavior of this mutant is the result of the removal of the conserved hydrophobic residues or the introduction of three additional positive charges. The importance of these hydrophobic residues is highlighted by the fact that mutant 4 has lower apoA-I levels and equivalent HDL-C levels as mutant 5 which lacks all residues beyond amino acid 219.

We have assessed the amount of loosely associated apoA-I by measuring the percentage of apoA-I in the lipid-free/lipid-poor fractions. The two mutants with the lowest plasma levels, mutants 4 and 5, also had the highest percent of total apoprotein in the lipid-free/lipid-poor state following density gradient centrifugation. The accumulation of lipid-poor mutant 5 apoA-I suggests that the reduced initial rate of association of mutant 5 with phospholipid observed in vitro (Figure 7) or limited association with preexisting HDL particles may prolong the half-life of the lipid-free/lipid-poor protein in the plasma. These raise the possibility that the C-terminal amino acids of apoA-I, aside from their role in lipoprotein association, may contain different overlapping domains that serve as signals for HDL catabolism. Of interest in this regard is the recent observation that mice lacking ABC A1 have much lower plasma apoA-I levels than any of the mutants examined in this study, even mutant 5 (*40*). Relatively little is known about the mechanisms of apoA-I loss from the plasma. It is generally believed that apoA-I not associated with lipoproteins is rapidly catabolized by the kidney (*41*) via the cubilin/megalin receptor pair (*12*, *13*, *42*). It may be sufficient for the apoA-I to be loosely associated with HDL rather than exist as free apoprotein for it to enter the rapidly catabolized pool.

CONCLUSION

In summary, a number of apoA-I point mutants and a deletion mutant have been studied in vivo focusing on the effect of these mutations on HDL concentration, subclass distribution pattern, formation of spherical or discoidal particles, and the percentage of apoA-I in the lipid-poor/lipid-free fractions. Our studies have focused on those changes that have been introduced primarily in helices 9 and 10 of apoA-I and the random coil connecting them. The hydrophobic residues in the C-terminus seem to be required for association of apoA-I with lipids and lipoproteins and possibly for HDL formation, stability, and catabolism. Changes in this region may produce differing effects on the nature of the HDL formed and perhaps larger effects on plasma HDL-C and apoA-I levels. Most of these changes appear to operate at the level of lipoprotein formation, stability, and catabolism rather than apoA-I synthesis and secretion. A key finding of this study is that substitution of hydrophobic residues in the 211 to 229 region of apoA-I which diminish the binding of apoA-I to HDL and phospholipids in vitro prevent the maturation of discoidal to spherical HDL particles in vivo. Deletion of this region also leads to low HDL levels. Our studies suggest that individual residues within this domain may participate in these aspects of HDL metabolism. These studies show that plasma levels and the physiological functions of HDL may be exquisitely sensitive to apoA-I alterations. Such alteration of apoA-I in the general population may contribute to low HDL levels and thus predispose humans to atherogenesis.

ACKNOWLEDGMENT

The authors thank Yimei Chen for assistance in the preparation of the electron photomicrographs.

REFERENCES

1. Zannis, V. I., Kardassis, D., and Zanni, E. E. (1993) *Adv. Hum. Genet. 21*, 145−319.
2. Fielding, C. J., and Fielding, P. E. (1995) *J. Lipid Res. 36*, 211−228.
3. Fielding, C. J., Shore, V. G., and Fielding, P. E. (1972) *Biochem. Biophys. Res. Commun. 46*, 1493−1498.
4. Soutar, A. K., Garner, C. W., Baker, H. N., Sparrow, J. T., Jackson, R. L., Gotto, A. M., and Smith, L. C. (1975) *Biochemistry 14*, 3057−3064.
5. Fielding, C. J. (1999) in *Advances in Cholesterol Research* (Esfahani, M., and Swaney, J. B., Eds.) pp 271−314, Teford Press, NJ.
6. Bakria, A., Puchois, P., Ghalim, P., Torpier, N., Barbaras, G., Ailhaud, R., and Fruchart, J. C. (1991) *Atherosclerosis 87*, 135−146.
7. Brooks-Wilson, A., Marcil, M., Clee, S. M., Zhang, L.-H., Roomp, K., van Dam, M., Yu, L., Brewer, C., Collins, J. A., Molhuizen, H. O. E., Loubser, O., Ouelette, B. F. F., Fichter, K., Ashbourne-Excoffon, K. J. D., Sensen, C. W., Scherer, S., Mott, S., Denis, M., Martindale, D., Frohlich, J., Morgan, K., Koop, B., Pimstone, S., Kastelein, J. J. P., Genest, J., Jr., and Hayden, M. R. (1999) *Nat. Genet. 22*, 336−345.
8. Rust, S., Rosier, M., Funke, H., Real, J., Amoura, Z., Piette, J.-C., Deleuze, J.-F., Brewer, H. B., Duverger, N., Denefle, P., and Assmann, G. (1999) *Nat. Genet. 22*, 352−355.
9. Bodzioch, M., Orso, E., Klucken, J., Langmann, T., Bottcher, A., Diederich, W., Drobnik, W., Barlage, S., Buchler, C., Porsch-Ozcurumez, M., Kaminski, W. E., Hahmann, H. W., Oette, K., Rothe, G., Aslanidis, C., Lackner, J. J., and Schmitz, G. (1999) *Nat. Genet. 22*, 347−351.
10. Roghani, A., and Zannis, V. I. (1988) *J. Biol. Chem. 263*, 17925−17932.
11. Acton, S., Rigotti, A., Landschulz, K., Xu, S., Hobbs, H. H., and Krieger, M. (1996) *Science 271*, 518−520.
12. Kozyraki, R., Fyfe, J., Kristiansen, M., Gerdes, C., Jacobsen, C., Cui, S., Christensen, E. I., Aminoff, M., De la Chapelle, A., Krahe, R., Verroust, P. J., and Moestrup, S. K. (1999) *Nat. Med. 5*, 656−661.
13. Hammad, S. M., Stefanson, S., Twai, W. O., Drake, C. J., Fleming, P., Remaley, A., Brewer, H. B., Jr., and Argraves, W. S. (1999) *Proc. Natl. Acad. Sci. U.S.A. 96*, 10158−10163.
14. Segrest, J. P., Jones, M. K., De Loof, H., Brouillette, C. G., Vankatachalapathi, Y. V., and Anantharamaiah, G. M. (1992) *J. Lipid Res. 33*, 141−166.
15. Nolte, R. T., and Atkinson, D. (1992) *Biophys. J. 63*, 1221−1230.
16. Palgunachari M. N., Mishra, V. K., Loud-Katz, S., Phillips, M. C., Adeyeye, S. O., Alluri, S., Anantharamaiah, G. M., and Segrest, J. P. (1996) *Arterioscler. Thromb. Vasc. Biol. 16*, 328−338.
17. Minnich, A., Collet, X., Roghani, A., Cladaras, C., Hamilton, R. L., Fielding, C. J., and Zannis, V. I. (1992) *J. Biol. Chem. 267*, 16553−16560.
18. Holvoet, P., Zhao, Z., Vanloo, B., Vos, R., Deridder, E., Dhoest, A., Taverirne, J., Brouwers, E., Demarsin, E., Engel-

borghs, Y., Rosseneu, M., Collen, D., and Brasseur, R. (1995) *Biochemistry 34*, 13334−13342.
19. Ji, Y. and Jonas, A. (1995) *J. Biol. Chem. 270*, 11290−11297.
20. Morrison, J., Fidge, N. H., and Tozuka, M. (1991) *J. Biol. Chem. 266*, 18780−18785.
21. Allan, C. M., Fidge, N. H., Morrison, J. R., and Kanellos, J. (1993) *Biochem. J. 290*, 449−455.
22. Mishra, V. K., Palgunachri, M. N., Datta, G., Phillips, M. C., Lund-Katz, S., Adeyeye, S. O., Alluri, S., Segrest, J. P., and Anantharamaiah, G. M. (1998) *Biochemistry 37*, 10313−10324.
23. Schmidt, H. H.-J., Remaley, A. T., Stonik, J. A., Ronan, R., and Wellmann, A. (1995) *J. Biol. Chem. 270*, 5469−5475.
24. Holvoet, P., Zhao, Z., Deridder, E., Dhoest, A., and Collen, D. (1996) *J. Biol. Chem. 271*, 19395−19401.
25. Holvoet, P., Danloy, S., Deridder, E., Lox, M., Bernar, H., Dhoest, A., and Collen, D. (1998) *J. Clin. Invest. 102*, 379−385.
26. Laccotripe, M., Makrides, S. C., Jonas, A., and Zannis, V. I. (1997) *J. Biol. Chem. 272*, 17511−17522.
27. Borhani, D. W., Rogers, D. P., Engler, J. A., and Brouillette, C. G. (1997) *Proc. Natl. Acad. Sci. U.S.A. 94*, 12291−12296.
28. Williamson, R., Lee, D., Hagaman, J., and Maeda, N. (1992) *Proc. Natl. Acad. Sci. U.S.A. 89*, 7134−7138.
29. Rubin, E. M., Ishida, B. Y., Clift, S. M., and Krauss, R. M. (1991) *Proc. Natl. Acad. Sci. U.S.A. 88*, 434−438.
30. Cabana, V. G., Reardon, C. A., Wei, B., Lukens, J. R., and Getz, G. S. (1999) *J. Lipid Res. 40*, 1090−1103.
31. Reardon, C. A., Blachowicz, L., Watson, K. M., Barr, E., and Getz, G. S. (1998) *J. Lipid Res. 39*, 1372−1381.
32. O'Meara, N. M., Cabana, V. G., Lukens, J. R., Loharikar, B., Forte, T. M., Polonsky, K. S., and Getz, G. S. (1994) *J. Lipid Res. 35*, 2178−2190.
33. Kashyap, V. S., Santamarina-Fojo, S., Brown, D. R., Parrott, C. L., Applebaum-Bowden, D., Meyn, S., Talley, G., Paigen, B., Maeda, N., and Brewer, H. B., Jr. (1995) *J. Clin. Invest. 96*, 1612−1620.
34. Koppaka, V., Silvestro, L., Engler, J. A., Brouillette, C. G., and Axelsen, P. H. (1999) *J. Biol. Chem. 274*, 14541−14544.
35. Segrest, J. P., Jones, M. K., Klon, A. E., Sheldahl, C. J., Hellinger, M., De Loof, H., and Havey, S. C. (1999) *J. Biol. Chem. 274*, 31755−31758.
36. Segrest, J. P., Li, L., Anantharamaiah, G. M., Harvey, S. C., Liadaki, N. K., and Zannis, V. I. (2000) *Curr. Opin. Lipidol. 11*, 105−115.
37. Frank, P. G., and Marcel, Y. L. (2000) *J. Lipid Res. 41*, 853−872.
38. Gillotte, K. L., Zaiou, M., Lund-Katz, S., Anantharamaiah, G. M., Holvoet, P., Dhoest, A., Palgunachari, M. N., Segrest, J. P., Weisgraber, K. H., Rothblat, G. H., and Phillips, M. C. (1999) *J. Biol. Chem. 274*, 2021−2028.
39. Gorshkova, I. N., Liadaki, K., Gursky, O., Atkinson, D., and Zannis, V. I. (2000) *Biochem. 39*, 15910−15919.
40. McNeich, J., Aiello, R. J., Guyot, D., Turi, T., Gabel, C., Aldinger, C., Hoppe, K. L., Roach, M. L., Royer, L. J., de Wet, J., Broccardo, C., Chimini, G., and Francone, O. L. (2000) *Proc. Natl. Acad. Sci. U.S.A. 97*, 4245−4250.
41. Glass, C., Pittman, R. C., Keller, G. A., and Steinberg, D. (1985) *J. Biol. Chem. 260*, 744−750.
42. Hammad, S. M., Barth, J. L., Knaak, C., and Argraves, W. S. (2000) *J. Biol. Chem. 275*, 12003−12008.

BI011451E